Quantitative Analysis of Amyloid-Integrated Biofilms Formed by Uropathogenic *Escherichia coli* at the Air-Liquid Interface

Cynthia Wu,[†△] Ji Youn Lim,[‡△] Gerald G. Fuller,[†] and Lynette Cegelski[‡*]
[†]Department of Chemical Engineering and [‡]Department of Chemistry, Stanford University, Stanford, California

ABSTRACT Bacterial biofilms are complex multicellular assemblies, characterized by a heterogeneous extracellular polymeric matrix, that have emerged as hallmarks of persistent infectious diseases. New approaches and quantitative data are needed to elucidate the composition and architecture of biofilms, and such data need to be correlated with mechanical and physicochemical properties that relate to function. We performed a panel of interfacial rheological measurements during biofilm formation at the air-liquid interface by the *Escherichia coli* strain UTI89, which is noted for its importance in studies of urinary tract infection and for its assembly of functional amyloid fibers termed curli. Brewster-angle microscopy and measurements of the surface elasticity (G_s') and stress-strain response provided sensitive and quantitative parameters that revealed distinct stages during bacterial colonization, aggregation, and eventual formation of a pellicle at the air-liquid interface. Pellicles that formed under conditions that upregulate curli production exhibited an increase in strength and viscoelastic properties as well as a greater ability to recover from stress-strain perturbation. The results suggest that curli, as hydrophobic extracellular amyloid fibers, enhance the strength, viscoelasticity, and resistance to strain of *E. coli* biofilms formed at the air-liquid interface.

INTRODUCTION

The propensity of bacteria to associate with surfaces and with each other far exceeds their tendency to persist in suspension, living freely in a planktonic state (1,2). When associated with one another, bacteria commonly form a multicellular community referred to as a biofilm. Biofilms are characterized by a heterogeneous extracellular polymeric matrix that includes proteins and polysaccharides, and often exhibit resistance to antibiotics and host defenses. Bacterial biofilms play a significant role in the transmission and persistence of human disease, and have emerged as hallmarks of virulence in serious infectious diseases, including cystic fibrosis pneumonia, infective endocarditis, urinary tract infection, and infections of indwelling medical devices (3,4). Microbial fouling is also an industrial, environmental, and economic burden. Undesired biofilms form in drinking water, in oil pipelines, and on the hulls of ships, hindering the ships' movement through water (5). Biofilms also form on industrial surfaces in contact with food in food production and preparation facilities. This can lead to the dispersal of food-borne pathogens and outbreaks attributed to organisms such as Salmonella species, *Escherichia coli*, *Listeria monocytogenes*, and Pseudomonas species (6–9). To understand the function of biofilms and to develop new strategies to prevent biofilm formation and ablate existing biofilms, it is crucial to obtain improved biofilm models.

Model-building efforts are challenging because multiple determinants contribute to biofilm development, and their role in biofilm formation may vary depending on environmental conditions. We have been engaged in elucidating how bacterial amyloid fibers, termed curli, contribute to biofilm formation and function. Curli are assembled at the extracellular surface of *E. coli* and other Enterobacteriaceae, and mediate adhesion to mammalian and plant cells as well as to inert surfaces such as glass, stainless steel, and plastic (10–16). Curli also promote biofilm assembly and other community behaviors (17–19). Curli production is prevalent among pathogenic *E. coli* strains implicated in host pathogenesis and are typically associated with infections involving persistent biofilms, such as uropathogenic *E. coli* (UPEC), which is responsible for infections in the bladder and kidneys, and the enterohemorrhagic strain *E. coli* O157:H7, which is responsible for many food-borne outbreaks (18,20).

As is typical of many adhesins and biofilm components, curli are sufficient to promote adhesion and biofilm formation on surfaces such as plant leaves and plastic, but can be dispensable under certain conditions if alternate adhesive fibers or proteins are expressed. This reality is one of several factors that contribute to the appreciation that targeting biofilm formation may require a multipronged approach (21). An additional factor is the complex and dynamic coordination and regulation of the expression of distinct virulence factors as a function of time and location in a host or in the environment. Yet, curli are uniquely required for pellicle formation (i.e., biofilm formation at the air-liquid interface) by UPEC. UTI89 is a biofilm-competent UPEC strain that forms biofilms on agar, on plastic, and at the air-liquid interface. A UTI89 curli mutant, UTI89Δ*csgA*, which is unable to produce curli due to deletion of the major subunit of the fiber, cannot form a pellicle under any condition (22). Other fibers important to UPEC virulence, such as type 1 pili, are not sufficient to permit pellicle formation (22). In

Submitted February 8, 2012, and accepted for publication June 27, 2012.

△Cynthia Wu and Ji Youn Lim contributed equally to this work.

*Correspondence: cegelski@stanford.edu

Editor: Ka Yee Lee.

0006-3495/12/08/0464/8 $2.00

http://dx.doi.org/10.1016/j.bpj.2012.06.049

addition, functional amyloid fibers composed of the TasA protein were recently reported to be required for *Bacillus subtilis* pellicle formation (23). Therefore, studying pellicle formation offers a unique opportunity to examine the contributions of amyloids to biofilm formation and function.

In a previous study (24), we discovered that moderate concentrations of dimethyl sulfoxide (DMSO) and ethanol (EtOH) upregulate curli protein production and fiber assembly, and increase UPEC biofilm formation on plastic (measured by a quantitative crystal violet assay) and at the air-liquid interface (assessed qualitatively by visual inspection). Microarray analyses identified a dramatic and selective upregulation in curli gene transcription that resulted in enhanced phenotypes (24). Overall, this discovery emphasized the significance of functional amyloid fibers and the ability of *E. coli* to enhance amyloid production, alter biofilm composition, and increase cohesion. However, the detected molecular and structural changes did not reveal how untreated and solvent-treated biofilms differ at the physicochemical level or how the mechanical properties of the biofilms differ. Ultimately, these properties will help us understand what makes one biofilm-former more robust, or more resistant to dispersal and eradication, than another one. By using DMSO and EtOH to increase curli production in the same bacterial strain, one can obtain comparative biofilm measurements that relate to molecular composition.

Conventional assessments of pellicle formation generally involve visual inspection of film formation at the air-liquid interface, confocal microscopy to assess obvious changes in overall thickness or topology, identification of proteins or components present in the pellicle using antibodies and dyes or mass spectrometry and proteomics approaches, and/or profiling of gene expression within cells in the film. Given the importance of biofilm formation and the ability of many pathogenic bacteria to form a pellicle, investigators have implemented more quantitative methods to examine the physicochemical properties of a pellicle. A recent study of *Pseudomonas fluorescens* included measurements of surface tension and rheological parameters to assess the fragility and viscoelasticity of a pellicle in the absence and presence of iron, which is associated with increased cellulose production (25). Similarly, the influence of other chemical perturbations on mechanical properties at the air-liquid interface was examined in biofilms formed by *P. aeruginosa*, the pathogen associated with chronic lung infections in patients with cystic fibrosis (26).

In this work we integrated a unique panel of assays, including electron microscopy, Western blotting, and rheological measurements, to fully characterize the formation of pellicles by UPEC. In particular, to obtain sensitive and quantitative parameters, and to correlate pellicle features with fundamental physicochemical properties and function, we employed Brewster-angle microscopy (BAM) and interfacial shear rheometry to study changes in viscoelasticity and surface aggregation as a function of time during amyloid-integrated *E. coli* pellicle formation. Our data reveal the presence of distinct stages in pellicle formation and identify differences among biofilms formed with altered amyloid content. The results provide a correlation of molecular composition with function and show that increased amyloid production provides increased interfacial viscoelasticity and an increased ability to recover from mechanical strain.

MATERIALS AND METHODS

Pellicle assay

The UPEC isolate UTI89 and its isogenic *csgA* mutant, UTI89Δ*csgA*, were grown in YESCA (0.5 g/L yeast extract, 10 g/L casamino acids) broth containing either no added solvent or 2% DMSO, 4% DMSO, or 2% EtOH in 24-well-plate wells or in 50-ml conical tubes at 26°C without shaking. Pellicle formation was evaluated at 24, 48, and 72 h of incubation. Comparative growth curves of planktonic cells during pellicle formation were obtained by measuring the optical density at 600 nm of bacterial cultures. Total bacterial cell numbers (cfu/ml) were also enumerated after 24 h incubation with 200 rpm shaking at 26°C.

BAM

To characterize pellicle formation and early assembly of aggregates at the air-liquid interface, we used a Brewster-angle microscope (27,28). The laser and the CCD camera were placed at the Brewster angle to the liquid surface. The 12-well plate (well diameter: 22.11 mm) was used for BAM. Bacteria from overnight starter cultures grown in YESCA broth were added to fresh YESCA broth with or without DMSO or EtOH (1:1000), and the diluted bacterial culture was added to the well until the reflection of the laser beam from the liquid surface was detected by the CCD camera. Videos of the surface were recorded at various time points, and images were extracted and analyzed.

Scanning electron microscopy

For scanning electron microscopy (SEM), pellicle samples were prepared after 5 days of incubation at 26°C in YESCA broth with or without 4% DMSO or 2% EtOH in 50-ml conical tubes. Each pellicle sample was treated with a fixation solution (2% glutaraldehyde and 4% formaldehyde in 0.1 M Na-Cacodylate, pH 7.4) overnight at 4°C. After fixation, each pellicle was washed with 0.1 M Na-Cacodylate buffer (pH 7.4) for 10 min with shaking, and then post-fixed with 1% aqueous osmium tetroxide in 0.1 M Na-Cacodylate buffer (pH 7.4) for 90 min. Each pellicle was then washed again and dehydrated using successive 50%, 70%, 95%, and 100% EtOH treatments, each for 10 min. Finally, the residual EtOH of each dehydrated pellicle was removed with a critical point dryer, and the samples were coated with gold-palladium. A Hitachi S-2400 N scanning electron microscope was used for acquisition of all images.

Interfacial rheometry

The viscoelastic dynamics of each pellicle was measured with the use of an AR-G2 rheometer (TA Instruments, New Castle, DE) with a du Noüy ring and a double-wall Couette Teflon flow-cell apparatus (Fig. 1) (29). To initiate pellicle formation, 9.6 mL of a 1:1000 dilution of an overnight culture in fresh YESCA media containing DMSO or EtOH were prepared and added to a double Couette Teflon flow-cell apparatus. A 5-ml syringe

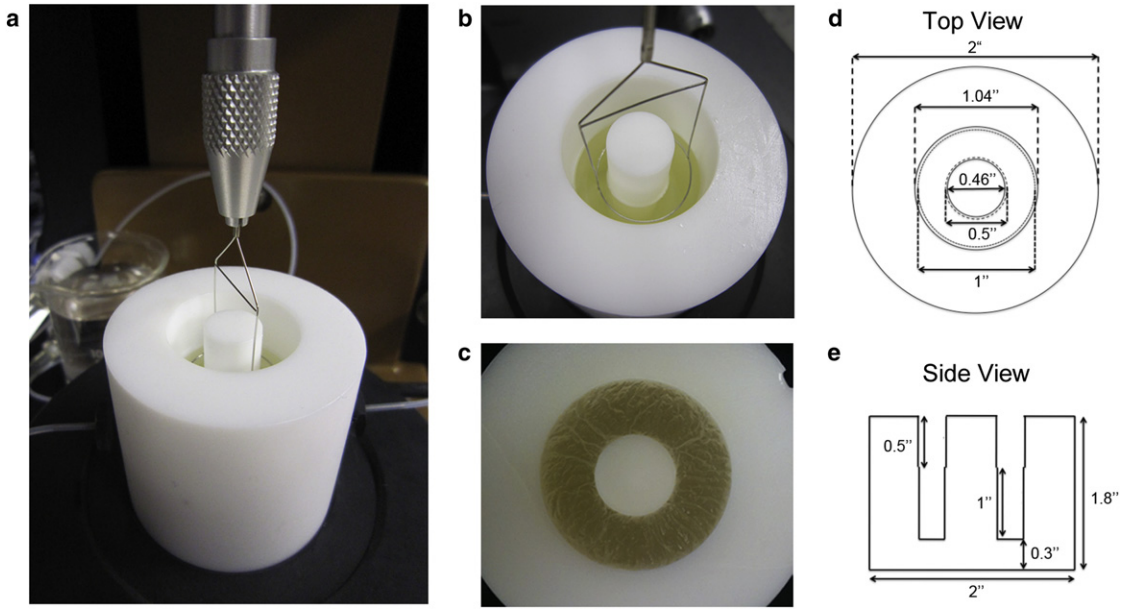

FIGURE 1 (*a*) The AR-G2 Rheometer with a Du Noüy ring and a double Couette teflon flow cell apparatus. (*b*) Close-up of the Du Noüy ring positioned in the air-liquid interface. (*c*) Pellicle formed in a double-couette teflon flow cell apparatus without a Du Noüy ring. (*d* and *e*) Schematic diagram showing top (*d*) and side views (*e*) of a double Couette teflon flow cell apparatus. Note the ports in the lower portion of the cell that allow the flow of solutions into and out of the subphase. This allows maintenance of the height of the interface and the concentrations within the subphase.

filled with fresh medium was connected through tubing to the bottom side of the flow-cell apparatus. The syringe was controlled by a syringe pump to inject fresh media continuously into the flow cell at a rate of 0.032 ml/h to replenish the media lost due to evaporation during the course of the experiment. A du Noüy ring made of thin Pt/Ir wire was positioned in the plane of the air-liquid interface in the flow-cell apparatus. The ring oscillated at 0.5 rad/s angular frequency with a strain of 1% about its circular axis for 72 h. After 72 h, a strain sweep at 0.5 rad/s angular frequency was performed. The applied strain was increased until the region of linear viscoelasticity was surpassed and the moduli were observed to decrease (this occurred at ~30% strain). After the strain sweep, the surface was monitored for 24 h at 0.5 rad/s and a strain of 1% to monitor the extent of restoration of the pellicle.

RESULTS AND DISCUSSION

Evolution of surface morphology and pellicle initiation by BAM

In a previous study (24), DMSO- and EtOH-induced upregulation of curli production was revealed by electron microscopy and immunoblot-based protein profiling for UTI89 and other UPEC strains growing under standard laboratory conditions on agar and in both static and shaking nutrient broth. Curli production was shown to be tunable over a range of solvent concentrations. A maximal increase in curli production was observed in the presence of 4% DMSO and 2% EtOH. The influence of DMSO solvent was studied in more detail because it had a selective effect on curli gene upregulation, whereas EtOH induced many global transcriptional changes associated with the well-studied but complex response to EtOH stress (27). In particular, more curli were produced in medium supplemented with 4% DMSO compared with 2% DMSO. Together with one EtOH-treated sample, this provided a useful pair for comparison in this study. Enhanced and tunable biofilm formation on plastic was noted, and mature pellicles grown in the presence of 2% DMSO, 4% DMSO, and 2% EtOH appeared more physically robust than nontreated pellicle, as assessed by perturbation with a pipette tip (24). However, due to the nonquantitative nature of the pellicle assay, further distinction of the samples was not possible. In addition, pellicle production (or lack thereof) is typically reported when a mature pellicle has formed (or not formed) after 3–5 days of incubation. Significant differences were not detected by visual inspection during the first 2–3 days of pellicle formation (24). To understand the influence of curli on community behavior and pellicle formation, we need to develop alternative and sensitive techniques to assess functional phenotypes and the consequences of increased amyloid content among biofilms.

In the work presented here, we employed BAM to examine pellicle formation with higher sensitivity than can be achieved by visual inspection as a function of time. BAM is a technique that allows the in situ study of thin films at gas-liquid or solid-gas interfaces. BAM images were acquired during pellicle formation of UTI89 growing in treated or untreated medium in separate 12-well-plate wells. Aggregates exhibiting a higher reflection were observed as white objects in the images (Fig. 2 *a*). Aggregates at the air-liquid interface appeared earliest among the 4%

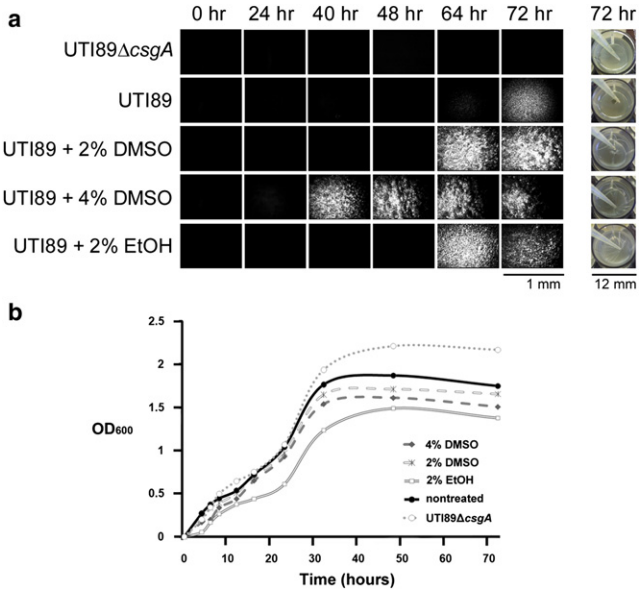

FIGURE 2 (*a*) BAM images of pellicle formation as a function of time. BAM images tracking pellicle formation for each condition were obtained from bacteria growing in a 12-well-plate well at room temperature in the presence and absence of DMSO or EtOH. Surface aggregates were detected first (at 40 h) in the 4% DMSO-treated UTI89 sample. Photographs of each mature pellicle, after a 72-h growth period, are presented in the rightmost column. (*b*) Growth curves of planktonic bacteria underlying the pellicle. Aliquots of planktonic cells beneath the pellicle were assayed by spectrophotometry (OD_{600}). The more robust pellicle-forming conditions, with added DMSO or EtOH, were accompanied by lower planktonic cell growth compared with the nontreated UTI89 pellicle. UTI89Δ*csgA* did not form a pellicle, and reached the highest planktonic cell density among the samples.

DMSO-treated pellicle-forming bacteria and were readily detected at 40 h. In the 2% DMSO- and 2% EtOH-treated wells, aggregates were observed clearly at 64 h. Some aggregates were visible at 64 h among the nontreated bacteria, but were more evident after 72 h. As anticipated, aggregates were not observed for the curli mutant, because UTI89 pellicle formation is curli dependent. These measurements reveal that DMSO and EtOH treatment influenced the timing of the inception of pellicle-associated aggregate formation.

We expected that overall bacterial growth under the conditions tested would be unaltered, because the same concentrations of DMSO and EtOH had no influence on growth rate or cell viability when samples were grown in standard laboratory conditions, with shaking in broth (24). In addition, if bacteria have an increased propensity to aggregate and to continue to replicate at the air-liquid interface, this phenomenon should be matched by a decrease in planktonic bacterial cell number beneath the surface over the course of pellicle formation. Thus, we initiated an additional round of pellicle formation and monitored the optical density of the underlying cells (Fig. 2 *b*). UTI89Δ*csgA* did not form a pellicle and reached the highest optical density of the sample set. A decrease in optical density was observed for UTI89 cells in the subphase, consistent with the enhanced propensity of bacteria to localize to the cell surface during formation of a pellicle. Further decreases in optical density were observed among the solvent-treated samples, as expected.

BAM is noninvasive, and the BAM images revealed detectable differences in the temporal aspects of bacterial aggregation as pellicle formation was initiated. The concomitant decreases in optical density data obtained by spectrophotometry paralleled the increased aggregation propensity and film formation at the surface, and should be of value for routine studies of pellicle formation by other UPEC and other organisms.

Topography of mature pellicles by SEM

Inspired by the differences we observed in the BAM images, we visualized mature pellicles by SEM. Previously reported images at submicron resolution revealed increased curli content on individual bacteria. In this study, we were interested primarily in the influence of community behavior on bulk surface properties that influence function at the air-liquid interface. Therefore, we imaged large sections of intact mature pellicles to examine whether the overall pellicle topology could be distinguished by SEM. From the images, we did not detect significant differences among the untreated and treated pellicles at low magnification, but we did observe increased curli production and extracellular matrix material in solvent-treated samples at higher resolution (Fig. 3). The SEM images also revealed a distinction between the air and liquid surfaces of the pellicle (Fig. 3). The liquid side of each pellicle was observed as smoother and more film-like in appearance, whereas the larger build-up of three-dimensional structures with large mounds and grooves was associated with the air-exposed surface. Thus, these images provide higher-resolution details of mature pellicles, although they require sample perturbation via removal from the pellicle-formation compartment. Curli protein production was also profiled in the three pellicle samples by Western blot analysis (Fig. S1 in the Supporting Material), and the results confirmed that curli protein production was increased in the presence of DMSO and EtOH during pellicle formation.

Progression of the surface elastic modulus during pellicle formation and stress

The above results show that BAM is valuable for identifying temporal differences to facilitate the detection of biofilm-like cellular aggregates at the air-liquid interface. We sought to obtain additional parameters with the sensitivity and comparative power to reveal the physicochemical nature of the pellicle assembly process that leads to observable aggregates and, eventually, a film at the air-liquid interface. Interfacial rheology techniques have been developed to

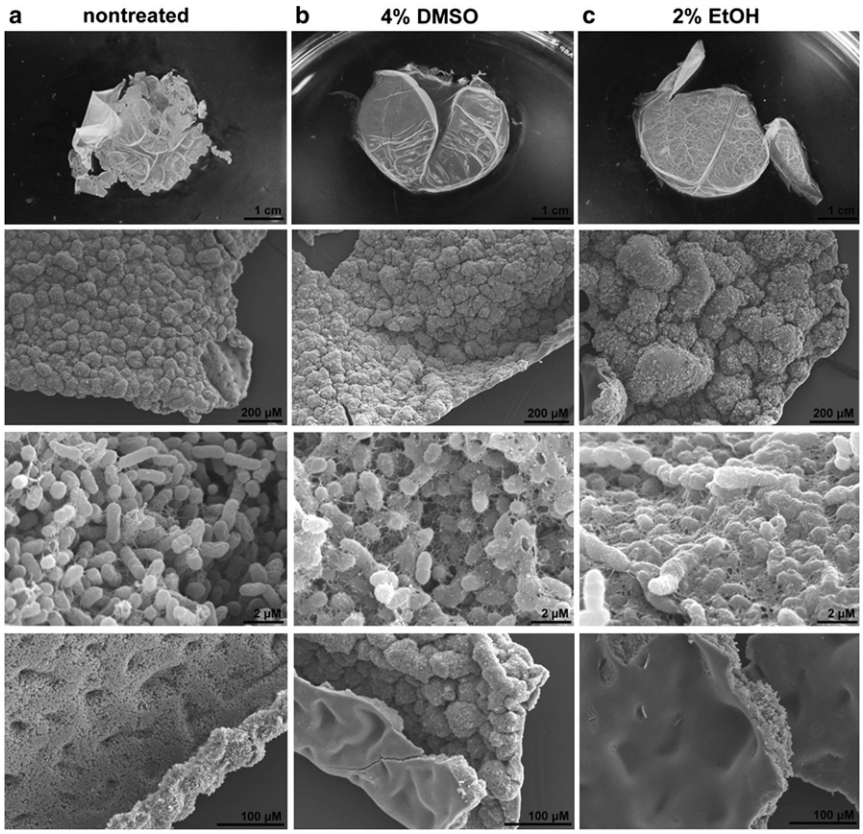

FIGURE 3 SEM images of mature pellicles. The top row shows photographs of the harvested pellicles before sample fixation. SEM images of the pellicles reveal details of the surface topology of mature pellicles formed over 5 days at 26°C in YESCA broth (*a*), and YESCA broth containing 4% DMSO (*b*) or 2% EtOH (*c*) at low magnification (*second row*) and higher magnification (*third row*). The increased curli production among bacteria in the DMSO- and EtOH-treated samples is apparent in the highest-resolution images in the third row. The electron micrographs in the bottom row reveal the distinction between the rough air-facing and smoother liquid-facing sides of the pellicle.

determine the mechanical response of complex fluid interfaces as reflected through various material functions, such as frequency-dependent, interfacial moduli. Such measurements can be acquired along with measurements of thermodynamic variables (e.g., surface tension). Thus, these techniques are crucial for characterizing polymer thin films and coatings (30), examining the roles of lung surfactants that decrease surface tension crucial to breathing (31), understanding tear film stability and proper hydration of the eye (32), and examining other complex fluid interfaces in biology, medicine, and industrial science (33).

To obtain G_s' measurements, we built a pellicle-formation chamber made of Teflon that contained a subsurface portal to allow the nonperturbative addition of liquid nutrient broth to minimize changes in the pellicle position or height due to evaporative loss over the course of multiple-day time-course experiments (Fig. 1 *a*). We measured the surface elastic modulus by measuring the torque and angular displacement of a du Noüy ring made of thin Pt/Ir wire that was positioned in the plane of the air-liquid interface and oscillated at a constant angular frequency (0.5 rad/s) with a defined strain of 1% about its circular axis for 72 h. This method allows sensitive determinations of surface moduli at very low applied strain and can be conducted without significant disturbance of the sample. Both the viscous and elastic interfacial moduli were recorded as functions of time. Although the air-liquid interfaces were initially more viscous than elastic, the surface elastic moduli quickly grew to overtake the surface viscous moduli, as shown in Fig. 4 *a* for the case of UT189 evolving in the absence of DMSO or EtOH. Measurements of the interfacial elastic modulus were made during pellicle formation in the presence and absence of DMSO or EtOH (Fig. 4 *b*). The data for four comparative pellicle-formers are compared in Fig. 4 *b* with those for the curli mutant, UTI89Δ*csgA*, which does not form a pellicle. The data provided in Fig. 4 *b* are representative of three independent measurements of three samples corresponding to each condition.

The progression of the interfacial modulus of each pellicle-former exhibited an overall profile that consisted of two rise-and-plateau stages. The profiles were similar at early time points. The first rise corresponds to the development of interfacial viscoelasticity attributed to components in the nutrient medium (most likely protein in the yeast extract) (34) and an increase in the cell density at the surface (Fig. 4 *a*), consistent with the turbidity data in Fig. 2. The first plateau occurred 10–20 h after inoculation, as the bacteria approached the stationary phase in static broth (Fig. 4 *a*). UTI89Δ*csgA* reached this first plateau but did not exhibit any further increase in G_s'. Therefore, the early contributions to the interfacial modulus appear to be curli independent. After 15–20 h, as cells entered the stationary phase,

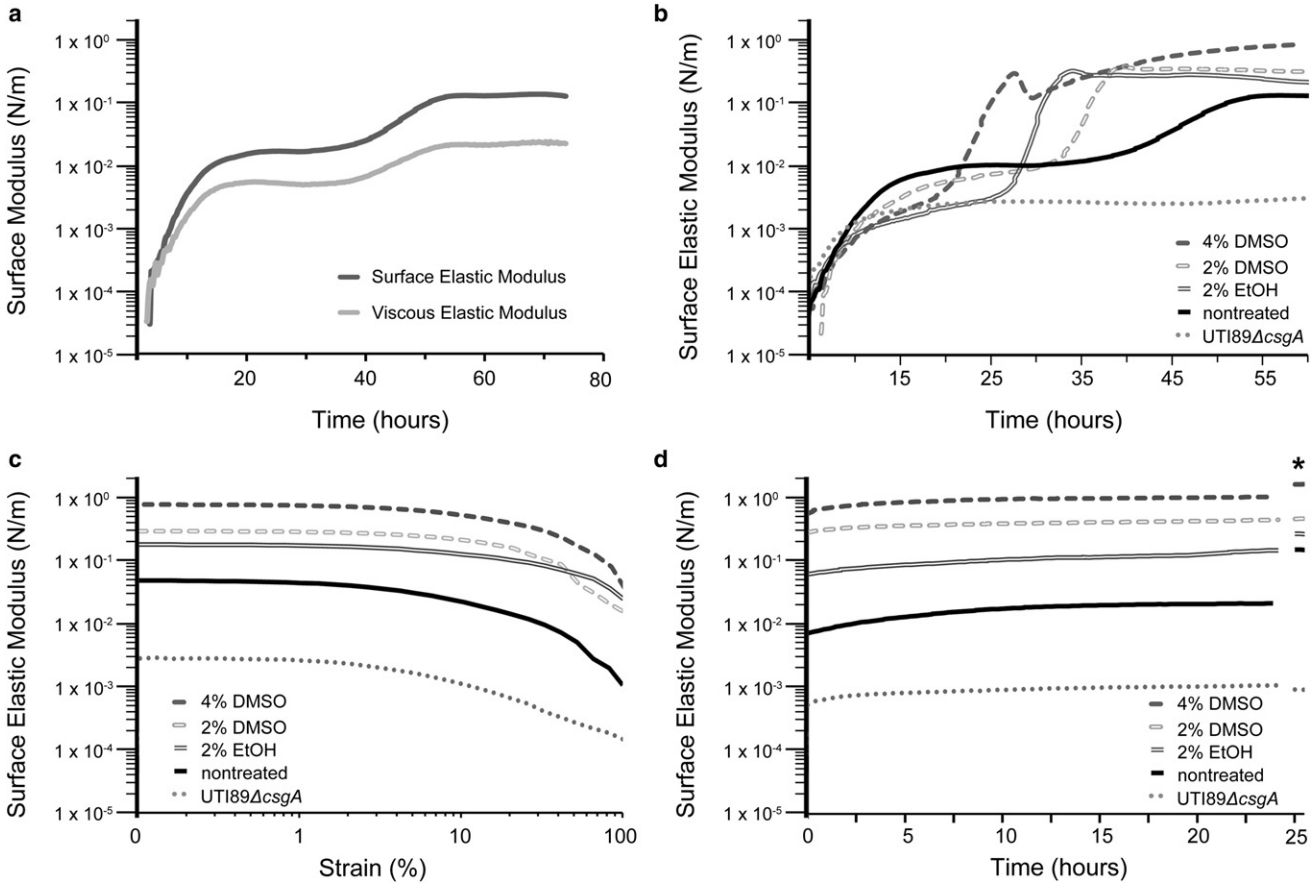

FIGURE 4 Measurement of the dynamic viscoelastic modulus during pellicle formation. (*a*) The surface elastic (G_s') and viscous (G_s'') moduli of UTI89 exhibit similar changes throughout the experimental period. The surface elastic modulus (G_s') increased in the presence of DMSO or EtOH. (*b*) UTI89Δ*csgA* did not exhibit the second rise associated with pellicle formation. (*c*) G_s' during strain sweep from 0 to 100% strain. (*d*) G_s' recovery after strain degradation of the pellicle. The asterisk indicates the G_s' value before strain sweep from *a*.

the three curli-enhanced pellicle samples exhibited a dramatic increase in G_s'. The increase in G_s' for untreated UTI89 pellicle formation was more modest and reached a final plateau of 0.13 N/m, which is considerably lower than the 0.84 N/m plateau reached by the UTI89 pellicle formed in the presence of 4% DMSO. In each case, we recorded this rise and plateau in G_s' before the formation of mature pellicles, as scored by visual inspection. Thus, although visible pellicles were not observed until much later (after 60 h), stable surface elastic moduli were reached between 40 and 60 h, depending on the sample. We also determined that an increase in G_s' could be achieved even when DMSO was added to the growing culture later in time, after cells had colonized the surface and reached the first plateau, although they did not reach as high a final G_s' value as when DMSO was present from the start of growth to promote the enhanced production of curli and curli-integrated biofilm formation (Fig. S2).

These data demonstrate that measurements of G_s' report in a sensitive way on surface elasticity, which is influenced by an increase in surface cell density and by changes associated with the commencement of film formation. To further assess potential differences in the strength and properties of the formed pellicles, we examined the response of the pellicles to induced mechanical strain. After 72 h of pellicle formation, at which point the pellicles resembled the Teflon-cell-grown pellicle in Fig. 1, each pellicle was subjected to strain sweep from 0 to 100% strain. As shown in Fig. 4 *b*, the pellicles did break down when subjected to sufficiently large strain, on the order of 10%. The films produced in the presence of DMSO are the most robust and exhibit the smallest diminution of the elastic surface modulus with strain. After the strain sweeps were completed, the surface elastic modulus of each pellicle was allowed to recover, and this was monitored as a function of time by recording G_s' at a strain of 1%. The recovery kinetics indicated that the pellicles recovered to an extent that depended on the amyloid content (Fig. 4 *c*). Pellicles that formed in the presence of 4% DMSO (associated with the highest curli production) exhibited the shortest time for regeneration and recovered to nearly the same G_s' value as measured before the strain. The strain-induced degradation of UTI89 in YESCA with no additive (the weakest curli producer among the pellicle formers) was the most

perturbative, and the prestrain G_s' value and viscoelastic property of the UTI89 pellicle could not be recovered after strain-induced degradation. Therefore, enhanced amyloid production during pellicle formation is associated with the ability of a pellicle to heal and regenerate itself after mechanical stress.

CONCLUSIONS

In this work, we examined pellicle formation under different conditions in a sensitive and quantitative manner using BAM and interfacial rheometry (G_s') to identify time-dependent stages during assembly of amyloid-integrated *E. coli* biofilms at the air-liquid interface, and to assess the functional consequences of increased amyloid content during assembly. We demonstrated that both BAM and G_s' are sensitive to the inception of biofilm formation, and that measurable signals are produced well before visual inspection of the interface reveals the presence of a film. However, the two measurements provide qualitatively different information regarding the contributions of curli to the biofilm. The G_s' measurements reveal distinct differences in the viscoelasticity associated with the enhanced network of amyloid fibers and appear to be more sensitive to the overall evolution of the film. We found that increased curli expression resulted in earlier detection of surface aggregates (by BAM) and yielded pellicles that were characterized by a higher surface elasticity and a significantly enhanced ability of the pellicle to recover from strain-induced disruption (by G_s'). Thus, our results enabled us to correlate molecular-level features with mechanical properties and biofilm function.

Our comparative analysis of samples in this study provides support for the notion that pellicle formation should be aided by the production of hydrophobic surface structures that enhance the propensity of bacteria to localize and assemble at the air-liquid interface rather than in the underlying nutrient broth. It is fascinating that curli (the hydrophobic structures) are amyloid fibers. When the soil-dwelling bacterium *Streptomyces coelicolor* egresses from its moist niche, it filaments, grows into the air, and forms spores. To promote this transition, *S. coelicolor* secretes amyloid-like fibers termed aerial hyphae or chaplins. Likewise, amyloid fibers composed of the protein TasA are required for *Bacillus subtilis* pellicle formation, and it is likely that future studies will identify amyloids in other organisms that function similarly. Typical proteins, which do not contain amyloid fibers, are often unstable and unfold at such interfaces (35,36). In general, however, it appears that curli and perhaps functional amyloids are produced by microbes that have harnessed the amyloid folding pathway to generate a very stable surface-associated fiber that promotes interfacial colonization and affords protection from desiccation, as suggested previously (37), and from mechanical strain, as demonstrated here.

The correlation of fundamental molecular and chemical properties with function is necessary to understand what makes one pellicle-former more or less robust than another, and our work demonstrates that curli content is correlated with pellicle strength. In addition, efforts are ongoing in our laboratory and others to identify and develop small-molecule inhibitors of amyloid formation and amyloid-integrated biofilm formation. Previously, successful inhibition of pellicle formation was determined by visual inspection, although there are many possible ways in which an inhibitor can prevent pellicle formation or promote the disassembly of an existing pellicle. Thus, even after a pellicle inhibitor is identified, it is important to understand the molecular and chemical basis of the inhibitor's action to drive the development of inhibitors with perhaps increased potency or other desired properties, as well as to overcome any inhibitor-resistance mechanisms that might emerge. The measurements presented here can be used to identify the particular stage of pellicle formation in which an inhibitor is working. The approach is also amenable to biofilm-disassembly studies in which the inhibitor is introduced after the formation of a pellicle. Our studies focused on UPEC, a human pathogen, but the method presented here can also be used to study amyloid-integrated biofilm formation in other organisms.

SUPPORTING MATERIAL

Supporting methods, two figures, and references are available at http://www.biophysj.org/biophysj/supplemental/S0006-3495(12)00775-8.

L.C. holds a Career Award at the Scientific Interface from the Burroughs Wellcome Fund. L.C. received support from the National Institutes of Health (Director's New Innovator Award 1DP2OD007488), Stanford University, and the Stanford Terman Fellowship. G.F. received support from the CBET Division of the National Science Foundation.

REFERENCES

1. Hall-Stoodley, L., J. W. Costerton, and P. Stoodley. 2004. Bacterial biofilms: from the natural environment to infectious diseases. *Nat. Rev. Microbiol.* 2:95–108.
2. Sand, W., and T. Gehrke. 2006. Extracellular polymeric substances mediate bioleaching/biocorrosion via interfacial processes involving iron(III) ions and acidophilic bacteria. *Res. Microbiol.* 157:49–56.
3. Hall-Stoodley, L., and P. Stoodley. 2005. Biofilm formation and dispersal and the transmission of human pathogens. *Trends Microbiol.* 13:7–10.
4. Parsek, M. R., and P. K. Singh. 2003. Bacterial biofilms: an emerging link to disease pathogenesis. *Annu. Rev. Microbiol.* 57:677–701.
5. Flemming, H. C. 2002. Biofouling in water systems—cases, causes and countermeasures. *Appl. Microbiol. Biotechnol.* 59:629–640.
6. Joseph, B., S. K. Otta, …, I. Karunasagar. 2001. Biofilm formation by salmonella spp. on food contact surfaces and their sensitivity to sanitizers. *Int. J. Food Microbiol.* 64:367–372.
7. Ryu, J. H., and L. R. Beuchat. 2005. Biofilm formation by *Escherichia coli* O157:H7 on stainless steel: effect of exopolysaccharide and curli production on its resistance to chlorine. *Appl. Environ. Microbiol.* 71:247–254.

8. Kumar, C. G., and S. K. Anand. 1998. Significance of microbial biofilms in food industry: a review. *Int. J. Food Microbiol.* 42:9–27.

9. Pan, Y., F. Breidt, Jr., and S. Kathariou. 2006. Resistance of *Listeria* monocytogenes biofilms to sanitizing agents in a simulated food processing environment. *Appl. Environ. Microbiol.* 72:7711–7717.

10. Uhlich, G. A., N. W. Gunther, 4th, …, D. A. Mosier. 2009. The CsgA and Lpp proteins of an *Escherichia coli* O157:H7 strain affect HEp-2 cell invasion, motility, and biofilm formation. *Infect. Immun.* 77:1543–1552.

11. Jonas, K., H. Tomenius, …, O. Melefors. 2007. Roles of curli, cellulose and BapA in *Salmonella* biofilm morphology studied by atomic force microscopy. *BMC Microbiol.* 7:70.

12. Barak, J. D., L. Gorski, …, A. O. Charkowski. 2005. *Salmonella enterica* virulence genes are required for bacterial attachment to plant tissue. *Appl. Environ. Microbiol.* 71:5685–5691.

13. Olsén, A., M. J. Wick, …, L. Björck. 1998. Curli, fibrous surface proteins of *Escherichia coli*, interact with major histocompatibility complex class I molecules. *Infect. Immun.* 66:944–949.

14. Ryu, J. H., H. Kim, and L. R. Beuchat. 2004. Attachment and biofilm formation by *Escherichia coli* O157:H7 on stainless steel as influenced by exopolysaccharide production, nutrient availability, and temperature. *J. Food Prot.* 67:2123–2131.

15. Vidal, O., R. Longin, …, P. Lejeune. 1998. Isolation of an *Escherichia coli* K-12 mutant strain able to form biofilms on inert surfaces: involvement of a new ompR allele that increases curli expression. *J. Bacteriol.* 180:2442–2449.

16. Pawar, D. M., M. L. Rossman, and J. Chen. 2005. Role of curli fimbriae in mediating the cells of enterohaemorrhagic *Escherichia coli* to attach to abiotic surfaces. *J. Appl. Microbiol.* 99:418–425.

17. Uhlich, G. A., P. H. Cooke, and E. B. Solomon. 2006. Analyses of the red-dry-rough phenotype of an *Escherichia coli* O157:H7 strain and its role in biofilm formation and resistance to antibacterial agents. *Appl. Environ. Microbiol.* 72:2564–2572.

18. Kikuchi, T., Y. Mizunoe, …, S. Yoshida. 2005. Curli fibers are required for development of biofilm architecture in *Escherichia coli* K-12 and enhance bacterial adherence to human uroepithelial cells. *Microbiol. Immunol.* 49:875–884.

19. Zogaj, X., W. Bokranz, …, U. Römling. 2003. Production of cellulose and curli fimbriae by members of the family Enterobacteriaceae isolated from the human gastrointestinal tract. *Infect. Immun.* 71:4151–4158.

20. Barnhart, M. M., and M. R. Chapman. 2006. Curli biogenesis and function. *Annu. Rev. Microbiol.* 60:131–147.

21. Flemming, H. C., and J. Wingender. 2010. The biofilm matrix. *Nat. Rev. Microbiol.* 8:623–633.

22. Cegelski, L., J. S. Pinkner, …, S. J. Hultgren. 2009. Small-molecule inhibitors target *Escherichia coli* amyloid biogenesis and biofilm formation. *Nat. Chem. Biol.* 5:913–919.

23. Romero, D., C. Aguilar, …, R. Kolter. 2010. Amyloid fibers provide structural integrity to *Bacillus subtilis* biofilms. *Proc. Natl. Acad. Sci. USA.* 107:2230–2234.

24. Lim, J. Y., J. M. May, and L. Cegelski. 2012. Dimethyl sulfoxide and ethanol elicit increased amyloid biogenesis and amyloid-integrated biofilm formation in *Escherichia coli*. *Appl. Environ. Microbiol.* 78: 3369–3378.

25. Koza, A., P. D. Hallett, …, A. J. Spiers. 2009. Characterization of a novel air-liquid interface biofilm of *Pseudomonas fluorescens* SBW25. *Microbiology.* 155:1397–1406.

26. Lieleg, O., M. Caldara, …, K. Ribbeck. 2011. Mechanical robustness of *Pseudomonas aeruginosa* biofilms. *Soft Matter.* 7:3307–3314.

27. Honig, D., and M. Dietmar. 1991. Direct visualization of monolayers at the air-water interface by Brewster angle microscopy. *J. Phys. Chem.* 95:4590–4592.

28. Hénon, S., and J. Meunier. 1991. Microscope at the Brewster angle: direct observation of first-order phase transitions in monolayers. *Rev. Sci. Instrum.* 62:936–939.

29. Vermant, J., S. Vandebril, …, P. Moldenaers. 2010. A double wall-ring geometry for interfacial shear rheometry. *Rheol. Acta.* 49:131–144.

30. Fuller, G. G., G. T. Gavranovic, and J. M. Deutsch. 2005. Two-dimensional melts: polymer chains at the air-water interface. *Macromolecules.* 38:6672–6679.

31. Kao, P. N., J. W. Anseth, …, D. Upadhyay. 2005. Lung surfactant gelation induced by epithelial cells exposed to air pollution or oxidative stress. *Am. J. Respir. Cell Mol. Biol.* 33:161–168.

32. Leiske, D. L., S. R. Raju, …, G. G. Fuller. 2010. The interfacial viscoelastic properties and structures of human and animal Meibomian lipids. *Exp. Eye Res.* 90:598–604.

33. Miller, R., and L. Liggieri. 2009. Interfacial Rheology. Brill, Leiden.

34. Nishimura, S. Y., G. M. Magana, …, G. G. Fuller. 2008. Effect of lysozyme adsorption on the interfacial rheology of DPPC and cholesteryl myristate films. *Langmuir.* 24:11728–11733.

35. Tronin, A., T. Dubrovsky, …, C. Nicolini. 1996. Role of protein unfolding in monolayer formation on air-water interface. *Langmuir.* 12:3272–3275.

36. Li, F. Y., J. M. Yuan, and C. Y. Mou. 2001. Mechanical unfolding and refolding of proteins: an off-lattice model study. *Phys. Rev. E Stat. Nonlin. Soft Matter Phys.* 63:021905.

37. White, A. P., D. L. Gibson, …, M. G. Surette. 2006. Thin aggregative fimbriae and cellulose enhance long-term survival and persistence of *Salmonella*. *J. Bacteriol.* 188:3219–3227.